

# MULTITEMPORAL IMAGE REGISTRATION BASED ON MULTIRESOLUTION DECOMPOSITION

*Registro de Imagens Multitemporais Baseadas em Decomposição Multiresolução*

**Leila M. G. Fonseca**<sup>1</sup>  
**Max H. M. Costa**<sup>2</sup>  
**Thales S. Korting**<sup>1</sup>  
**Emiliano Castejon**<sup>1</sup>  
**Felipe C. Silva**<sup>1</sup>

<sup>1</sup> **National Institute for Space Research – INPE**  
**Image Processing Division**  
C.P. 515, 12227-001, São José dos Campos (SP), Brazil  
{leila, tkorting, felipe, castejon}@dpi.inpe.br

<sup>2</sup> **State University of Campinas - Unicamp**  
**FEEC/DECOM**  
C.P. 6101, 13081-970 Campinas (SP), Brazil  
max@decom.fee.unicamp.br

## ABSTRACT

Image registration is the process of overlaying two or more images of the same scene taken at different times, from different viewpoints, and/or different sensors. With the increase in the number of images collected every day from different sensors, automated registration of multi-sensor, multi-spectral and multi-temporal images has become an important application. In this paper an efficient algorithm for the registration of multi-temporal images with similar spectral responses is proposed. The procedure relies on the gray level information content of the images and their local wavelet transform modulus maxima. The registration algorithm is performed at progressively higher resolutions, which allows for faster implementation and higher registration precision. For the matching process, a novel procedure for automatic point feature detection based on wavelet transform is presented. Moreover, an investigation about the performance of four similarity measures in the task of feature point matching for satellite images is also presented. The results show that the matching method based on correlation is efficient to register images of similar spectral responses even if multi-temporal changes are present. To overcome the presence of rotation angle between the images to be registered, a procedure to estimate this angle is performed before the matching process. Measurements of performance are provided, as well as extensive experimental results, to illustrate the qualitative performance of the registration algorithm. Images of different sensors and acquisition time are used in the experiments.

**Keywords:** Image Registration, Wavelet Transform, Matching, Feature Detection

## 1. INTRODUCTION

Agencies from all over the world have launched many earth observation systems of high resolution, multi-bands and multi-sensors. The analysis of multitemporal and multisensor remote sensing datasets acquired by these systems can be efficiently done if the data refer to a common geometry. The processing of images such that their corresponding pixels have the same geometry comprises registration or geocoding of the images.

The high resolution of the sensors means that the geometrical corrections and registration of these

images must be done with considerable precision. The increased volume of data motivates development of automatic or quasi-automatic registration systems. Development of automatic image registration methods is still a wide field of research, due to the need to use them with images which vary significantly in content, radiometry and geometry. The general approach to image registration consists of the following four steps (Fonseca and Manjunath, 1997):

1. Feature identification: identifies a set of relevant features in a pair of images, such as edges, line intersections, region contours, regions textures, etc.

2. Feature matching: establishes correspondence between the identified features. Thus, each feature in the *sensed image* must be matched to its corresponding feature in the *reference image*. Each feature is identified with a pixel location in the image. The corresponding points are usually referred to as *control points*.
3. Spatial transformation: determines the *mapping function* that can match all the points in the image using information about the *control points* obtained in the previous step.
4. Interpolation: resamples the *sensed image* using the mapping functions to bring it into alignment with the *reference image*.

In general, registration methods differ from each other in that they can combine different techniques for feature identification, feature matching, and mapping and interpolation functions. The most difficult step in image registration is obtaining the correspondence between the two sets of features. This task is crucial to the accuracy of image registration and much effort has been spent in the development of efficient feature matching techniques. Given the matches, the task of computing the appropriate mapping functions does not involve much difficulty. The interpolation process is also quite standard.

Generally, there are two classes of methods that can be used to register images: area based and feature based matching (Fonseca and Manjunath, 1996; Zitova and Flusser, 2003). Area based methods can be applied to spectrally similar images whilst feature based matching can be used more generally to register any pair of images. Several image registration methods have been proposed in the literature (Li *et al.* (1995), Govindu *et al.* (1998), Fonseca *et al.* (1998), Dare and Dowman, (2001), Kanade and Okutomi, (1994), Cole-Rhodes *et al.*, (2003)). Fookes *et al.* (2004) proposed extensions to Mutual Information (MI) based stereo matching in order to increase the robustness of the MI algorithm. Fedorov *et al.*, (2002) developed an operational system for automatic image registration, using three approaches found on literature (Kenney and Majunath, (2001), Fonseca *et al.*, (1998) and Li *et al.*, (1995)), including also techniques for mosaicking images.

In this paper we present an efficient approach for registration of multi-temporal images with similar spectral responses. The correlation coefficient is used as a similarity measure and only the best pairwise fittings among all pairs of feature points are taken as control points. A consistency checking step is also involved to eliminate mismatches. This way we have a reliable initial guess for the registration transformation which is a crucial phase in the process. The wavelet transform decomposition is used to extract feature points which are taken as control points and to decompose the images in different resolution levels. The algorithm is performed at progressively higher resolution, which

allows for faster implementation and higher registration precision.

The registration algorithm is very simple and easy to apply because it needs basically only one parameter. Because the matching is carried out only on the selected feature points and in a coarse-to-fine manner, a significant amount of computation is saved in comparison to traditional pixel-by-pixel searching methods. Due to the fact that the registration procedure uses the gray level information content of the images in the matching process it is more adequate to register images of the same sensor or with similar spectral bands. In spite of this, it has demonstrated technical feasibility for many images of forest, urban and agricultural areas from Thematic Mapper (TM-5), SPOT and radar sensors taken at different times.

In addition to the registration method presented, one of the main contributions of this paper is the procedure for point feature detection based on wavelet decomposition. The method automatically selects point features to be used in the matching process. It is very simple and reasonably efficient in terms of computational complexity. Moreover, an investigation about the performance of four similarity measures in the task of feature point matching for satellite images is also presented. The results show that the matching algorithm based on correlation is efficient to register images of similar spectral responses even when multi-temporal changes occur. In order to overcome the presence of rotation angle between the images to be registered, a procedure to estimate this angle is performed before the matching process.

The organization of the paper is as follows. In the next section we provide the reader with an introduction to wavelet transforms. In the subsequent sections, we discuss in detail each step of the registration algorithm. Following this we present some results of registering satellite images. Finally, we present some conclusions.

## 2. WAVELET TRANSFORMS

Although the Wavelet theory is well known in the literature, we will briefly describe it in order to facilitate the description of equations in the posterior sections. Interested readers can find more information on wavelets and the wavelet transform in Chui, (1992), Fliege (1994), Graps, (1995) and Mallat (1989a, 1989b, 1999).

Wavelets are functions that satisfy certain mathematical requirements and are used in representing data or other functions.

Let  $\psi \in L^2 \mathbb{R}^a$  be a complex valued function. If the function  $\psi \in L^2 \mathbb{R}^a$  satisfies

$$\int_{\mathbb{R}^a} \psi(x) dx = 0 \quad (1)$$

it may be called a basic wavelet or "mother wavelet". The families of functions

$$\psi_{a,b}(x) = \frac{1}{\sqrt{|a|}} \psi\left(\frac{x-b}{a}\right) \quad \text{with } a, b \in \mathbb{R}, a \neq 0 \quad (2)$$

generated from the "mother wavelet" under the operations of dilation (or scaling) by a factor  $a$  and translation in time by a parameter  $b$  form a wavelet family.

The continuous wavelet transform of a function  $f(x) \in L^2(\mathbb{R}^a)$  with respect to this family of wavelets is given by the convolution integral

$$W_a^\psi f(x) = \int_{-\infty}^{\infty} f(u) \psi\left(\frac{x-u}{a}\right) du \quad (3)$$

$$= f(x) \psi_a(x)$$

where  $\psi_a(x) = \frac{1}{\sqrt{|a|}} \psi\left(\frac{x}{a}\right)$ .

The wavelet can be interpreted as the impulsive response of a band-pass filter, and the wavelet transform of a function as a convolution of the function with the dilated filter responses (GRAPS, 1995).

In practice the scale  $a$  should be discretized. For a particular class of wavelets, the scale  $a$  can be sampled along a dyadic sequence  $a = 2^j$  with  $j \in \mathbb{Z}$ , without modifying the overall properties of the transform (Mallat and Zhong, 1992). The transform corresponding to dyadic values of  $a$  is called the discrete wavelet transform (DWT), given by

$$W_{2^j}^\psi f(x) = f(x) C \psi_{2^j}^a(x) \quad (4)$$

The wavelet transform of 1-D functions can be extended to the 2-D case. Let us consider a smoothing function  $\phi(x, y)$ , taken as the impulse response of a 2-D low-pass filter. The first order derivative of  $\phi(x, y)$  decomposed in two components along the  $x$  and  $y$  directions, respectively, are

$$\psi^1(x, y) = \frac{\partial \phi}{\partial x}(x, y)$$

$$\psi^2(x, y) = \frac{\partial \phi}{\partial y}(x, y) \quad (5)$$

and these functions can be used as wavelets.

For any 2-D function  $f(x, y)$ , the wavelet transform at scale  $a = 2^j$  defined with respect to these two wavelets has two components (Mallat and Hwang, 1992), given by

$$W_{2^j}^1 f(x, y) = f(x, y) C \psi_{2^j}^1(x, y)$$

$$= f(x, y) C \frac{\partial}{\partial x} \phi_{2^j}(x, y)$$

$$= 2^j \frac{\partial}{\partial x} f(x, y) C \phi_{2^j}^c(x, y)$$

and

$$W_{2^j}^2 f(x, y) = f(x, y) C \psi_{2^j}^2(x, y)$$

$$= f(x, y) C \frac{\partial}{\partial y} \phi_{2^j}(x, y) \quad (6)$$

$$= 2^j \frac{\partial}{\partial y} f(x, y) C \phi_{2^j}^c(x, y)$$

Therefore, these two components of the wavelet transform are proportional to the coordinates of the gradient vector of  $f(x, y)$  smoothed by  $\phi_{2^j}(x, y)$ . They characterize the singularities along  $x$  and  $y$  directions, respectively (Mallat and Hwang, 1992).

We define the function

$$M^D f(2^j, x, y) = \sqrt{C^2 \left[ W_{2^j}^1 f(x, y) \right]^2 + \left[ W_{2^j}^2 f(x, y) \right]^2} \quad (7)$$

which is the modulus of the wavelet transform at the scale  $2^j$ . One can prove that for wavelets defined by Equation 6,  $M^D f(2^j, x, y)$  is proportional to the magnitude of the gradient field (Mallat and Zhong, 1992).

The angle  $\alpha$  between the gradient vector of  $f(x, y)$  and the horizontal is given by

$$\alpha_{2^j}(x, y) = \tan^{-1} \left[ \frac{W_{2^j}^2 f(x, y)}{W_{2^j}^1 f(x, y)} \right] \quad (8)$$

This angle indicates locally the direction where the signal exhibits the sharpest variations.

### 3. FEATURE POINT DETECTION USING WAVELET TRANSFORM

This section presents a method to select automatically point features to be used in the matching process. The features are extracted with the use of the modulus maxima of the wavelet transform. Moigne, (1994), Djamdji, (1995) and Corvi and Nicchiotti, (1995) also use the wavelet transform to extract salient features in the images, which can be used in the registration process. Moigne, (1994) uses a percentage

(10%) of the total number in bands HL and LH of the wavelet decompositions to represent the significant features in the images. Djamdji, (1993) use the points in which wavelet coefficients *à trous* (BIJAOU and GIUDICELLI, 1991) are maximum. Corvi and Nicchiotti, (1995) use the points in which wavelet coefficients are maximum or minimum values. The matching processing is performed separately for maxima and minima features. Zheng and Chellappa, (1993) use Gabor decomposition for feature extraction, which is computationally more expensive and complex.

Differently, we use the local maxima of wavelet transform to extract point features in the image. Our implementation uses three filters G, L and H, derived from cubic spline function, whose coefficients are shown in Table 1. The two components of the wavelet transform in the  $x$  and  $y$  directions are used to calculate the gradient field. The edge information present in the high frequency subbands of the wavelet transform is instrumental to the point feature identification and matching processes. For the wavelet decomposition we use an algorithm proposed by Mallat and Zhong, (1992), which is rather efficient in terms of computation time. Memory reduction is an important factor in remote sensing image processing since the amount of data is very large.

TABLE 1- FILTERS CORRESPONDENT TO CUBIC SPLINE WAVELET

n	G	L	H
0	-0.00008	0.00003	0.0625
1	-0.01643	0.00727	0.2500
2	-0.10872	0.03118	0.3750
3	-0.59261	0.06623	0.2500
4	0.59261	0.79113	0.0625
5	0.10872	0.06623	
6	0.01643	0.03118	
7	0.00008	0.00727	
8		0.00003	

Let us call the image to be warped the *warp* image and the image to which the warp image will be reduced the *reference* image. We compute the discrete multiresolution wavelet transform ( $L$  levels) of the two images.

The wavelet decomposition of an image is similar to a quadrature mirror filter decomposition with the low-pass filter L and its mirror high-pass filter H (FLIEGE, 1994). We call LL, LH, HL and HH the four images created at each level of decomposition, as in (MOIGNE, 1994), where this decomposition is also used for the purpose of image registration. In the current implementation, filters G and L are used to calculate bands LH and HL, and filter H is used to calculate band LL. Band HH has not been used in our implementation.

The next phase aims to identify features that are present in both images in each level of the decomposition. Here we use the modulus maxima of the wavelet transform to detect sharp variation points which

correspond to edge points in the images. The LH and HL subbands at each level of the wavelet transform are used to estimate the image gradient. For the wavelet decomposition we use the filters given in Cheong *et al.*, (1992).

In the feature point selection process, in each level of decomposition, four steps are involved:

- Edge points extraction using the modulus of the wavelet transform;
- Selection of edge points localized in high contrast regions;
- Suppression of non-maximum local edge points.

In the first step, the reference and warp images are processed in  $L$  levels in the wavelet decomposition. In each resolution level, the modulus of the wavelet transform  $M_{2^j}$  and the angle  $\alpha_{2^j}$  images are calculated. A point  $P(x_0, y_0)$  in resolution level  $j$  is recognized as an edge if

$$M_{2^j}(x_0, y_0) > M_{2^j}(x, y) \quad (9)$$

where  $(x, y)$  belongs to the two nearest neighbors of  $P(x_0, y_0)$  in the direction to which the gradient vector  $\alpha_{2^j}$  points.

A thresholding procedure is applied on the wavelet transform modulus image in order to eliminate non-significant edge points. Thus, a point  $(x, y)$  is recorded only if

$$M_{2^j}(x_0, y_0) > \tau_{2^j} \quad (10)$$

where  $\tau_{2^j} = \beta \sigma_{2^j} + \mu_{2^j}$  is a constant whose initial value is defined by the user and  $\sigma_{2^j}$  and  $\mu_{2^j}$  are the standard deviation and mean of the wavelet transform modulus image at level  $2^j$ , respectively. The parameter  $\beta$  controls the number of feature points selected for the matching. Since the number of feature points increases at finer resolutions, the parameter  $\beta$  is also increased in the higher levels of decomposition in order to select the most significant feature points in the images. This condition eliminates weak edges and ensures a consistency of edges in all resolution levels. Therefore, if the edge is sufficiently strong, it will appear practically in all resolution levels. This parameter is defined by user.

Consider a window  $w_c \times w_c$  ( $w_c$  is an odd integer) of points centered in  $P(x_0, y_0)$ . Let  $\sigma_w$  be the standard deviation of the image values inside the window. Let  $CO(x_0, y_0)$  denote a contrast measure defined as (Gonzalez and Woods, 1992):

$$CO(x_0, y_0) = 1 @ \frac{1}{1 + \sigma_w} \quad (11)$$

In order to ensure that feature points are localized in high contrast regions, a point  $P(x_0, y_0^a)$  is recorded if and only if

$$CO(x_0, y_0^a) > T_w \quad (12)$$

where  $T_w$  is a given threshold above which the contrast measure is considered sufficiently large. This condition reduces the number of mismatched pairs in the matching process, which is discussed in the next section.

Finally, the local maxima are calculated as

$$M_{2^j}(x_0, y_0^a) = \max_{x,y \in 2^j V_p} M_{2^j}(x, y^a) \quad (13)$$

where  $V_p$  is a neighborhood of  $P(x_0, y_0^a)$ , defined as a window of  $w_p \times w_p$  points centered at  $P(x_0, y_0^a)$ . This condition ensures that the feature point is unique in its surrounding area.

#### 4. POINT MATCHING

In this section, we shall verify the correct matching of the selected feature point pairs in the reference and warp images. A correlation based matching measure is used in the matching process. The use of the correlation coefficient as a similarity measure is motivated by good results obtained in an experimental study. This study is briefly presented in the next section.

##### 4.1 Defining a similarity measure

Area based matching methods use similarity measures to compare windows of two images. Various similarity measures have been reported in the literature (Pratt, (1974), Barnea and Silverman, (1972), Khosravi and Schafer, (1996) and Brunelli and Messelodi, (1995)). Brunelli and Messelodi, (1995) have compared the correlation coefficient to similarity measures based on the  $L_1$  norm. In tasks involving face recognition, similarity measures based on the  $L_1$  norm outperformed the correlation measure. In order to verify the performance of some similarity measures in the task of feature points matching we have developed a comparative study with four similarity measures. These include the traditional correlation coefficient, the Gray Hit or Miss Transform (GHMT) (Khosravi and Schafer, 1996), the Sequential Similarity Detection (SSD), and one of the measures based on the  $L_1$  norm (L1G) proposed by Brunelli and Messelodi, (1995).

Let  $f$  and  $g$  be two grayscale images. Let  $t$  be a  $L \times K$  window of  $g$  centered at  $(m, n^a)$ , called a template. Let  $W = \{i, j : i=0, \dots, L-1, j=0, \dots, K-1\}$  be the support of  $t$ . The comparison between the template and a window of  $f$ , with support  $W$  and centered at  $(x, y^a)$ , is accomplished through similarity

measures. The following equations define the four similarity measures mentioned above.

##### Correlation Coefficient:

$$C(x, y^a) = \frac{\sum_{i,j \in W} (f(x+i, y+j) - \mu_f)(t(i, j) - \mu_t)}{\sqrt{\sum_{i,j \in W} (f(x+i, y+j) - \mu_f)^2 \sum_{i,j \in W} (t(i, j) - \mu_t)^2}} \quad (14)$$

where  $\mu_f$  and  $\mu_t$  are the local means (average intensity values) of  $f$  and  $t$ , respectively.  $W$  is the support of template  $t$ , and  $L \times K$  is the cardinality of  $W$

The Gray Hit or Miss Transform (GHMT):

$$M(x, y^a) = \min_{i,j \in W} |f(x+i, y+j) - t(i, j)| \quad (15)$$

Sequential Similarity Detection (SSD):

$$S(x, y^a) = \sum_{i,j \in W} |f(x+i, y+j) - t(i, j)| \quad (16)$$

$L_1$  Norm (L1G):

$$G(x, y^a) = 1 - \frac{\sum_{i,j \in W} |f(x+i, y+j) - t(i, j)|}{L \times K} \quad (17)$$

where  $f$  and  $t$  are normalized values and  $G(x, y^a) \in [0, 1]$ .

We have investigated the performance of these measures in the task of feature point matching for actual satellite images. In the experiment, we selected 6 pairs of multitemporal images of size  $512 \times 512$  pixels: two of urban, two of forest and two of agricultural areas. These images were selected for the diversity of information that they presented, allowing for a more robust validation. The images were decomposed in two resolution levels and the matching process was accomplished in the lowest resolution level of the LL band. This procedure was adopted because it simulates the way in which the proposed registration algorithm is implemented.

One way to validate a measure of similarity is by quantifying its ability to detect correct matches. The larger the number of correct matches the better the performance of the corresponding similarity measure. When we use the correlation coefficient, for instance, to compare two features, the maximization of this measure for selecting the best match does not assure that the match obtained is correct. Although the correlation value is maximum, their low absolute values may lead

to false matched points. In this case, we say the matching has low confidence. Problems such as noise, occlusion and low contrast in the images can lead to mismatches. The absolute value of the correlation coefficient itself may be used as a meaningful confidence measure. Thus, a pair of feature points will be matched if the absolute value of the correlation coefficient is larger than a certain threshold. To validate the measures of similarity, we quantify their capacity to detect correct matches. A good similarity measure is one which gives very little or no false alarms and a minimum number of misses in the matching process. A false alarm is defined as a false match declared as valid, whereas a miss is defined as a valid match declared as false.

The experimental investigation has shown that the correlation coefficient outperformed the other methods for the chosen set of parameters. Fig. 1 plots the percentage of correct matches against the size  $M$  of the matching window for all methods. One can observe that GHMT method presents some oscillations with a salient peak around  $M=13$ . This behavior indicates a certain sensitivity of this method with respect to the window size. The correlation and  $L1G$  methods present similar performances and outperform the other methods, mainly for window sizes 6 or greater.

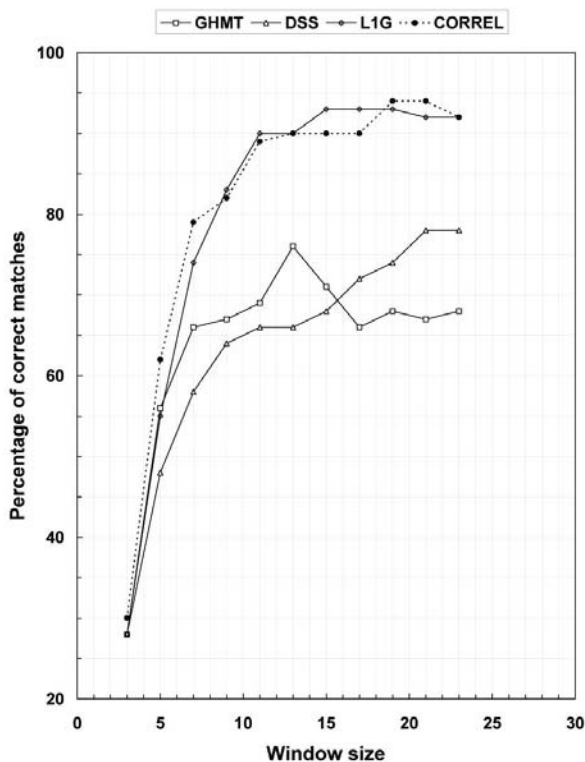


Fig. 1 – Performance of four matching methods with respect to matching window size: correlation coefficient (dashed line), GHMT, SSD, and  $L1G$ .

Fig. 2 shows the percentage of false alarms against the number of correct matches with window size  $M=13$  for the correlation and  $L1G$  methods. One can observe that correlation still slightly outperforms  $L1G$ .

It must also be considered that the  $L1G$  method is computationally more intense than the correlation method. Based on these evidences, the correlation coefficient measure demonstrated good robustness and efficiency. Therefore, it was chosen for use in the proposed registration method.

It is known that area based matching methods are very sensitive to rotation. Zheng and Chellappa, (1993) and Hsieh, (1997) have proposed different approaches to overcome this problem. Zheng and Chellappa, (1993) use a shape-from-shading technique to estimate the illuminant directions of images under the assumption that the illumination source is stationary. By taking the difference between the illuminant directions, the rotation angle between images can be estimated. Hsieh, (1997) uses a line-fitting model to estimate the directions of all the edges from the wavelet transform maxima. In order to estimate the orientation differences between the images, a so-called “angle histogram” is calculated. Then, the rotation is found by seeking the angle that corresponds to the maximum peak in the histogram. Both methods have drawbacks. As pointed out by Hsieh (1997), Zheng and Chellappa's approach does not work satisfactorily if the scene includes many buildings and objects due the fact that the illumination conditions in one image may not be equivalent to those in the other. On the other hand, Hsieh's method can fail if the changes between the images are reasonable high.

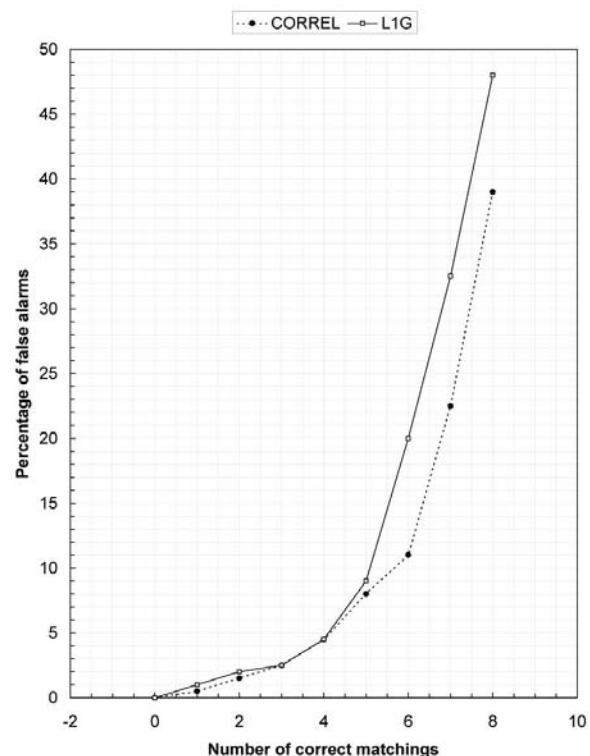


Fig. 2 – False alarm rate versus number of correct matches for correlation coefficient and  $L1G$  methods (with  $M=13$ ).

The method proposed in this paper aims mainly at registering remote sensing images, and the angle of rotation between satellites can be readily obtained as auxiliary information. If it is not the case, the proposed

scheme estimates the rotation angle by choosing windows about each feature point that have been rotated so that their central gradient points downward (Kenney and Manjunath, 2001).

#### 4.2 Initial Point Matching

The feature matching process is performed through a combination of area and feature based techniques. Fig. 3 shows the block diagram and the steps involved in the initial matching process. The feature point matching is achieved by maximizing the correlation coefficient over small windows surrounding the feature points within the LL subbands of the wavelet transform. Let the LL subbands of the warp and reference images be  $f_s$  and  $f_r$ , respectively, and let  $C_{f_s, f_r}(x, y, X, Y)$  be the corresponding correlation coefficient.

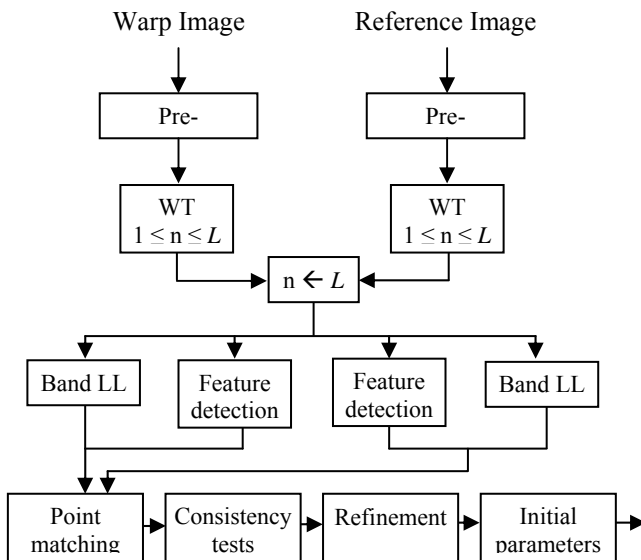


Fig. 3 – Initial Matching Process.

The initial matching is performed at the lowest resolution images and is determined by the best pair wise fitting between the feature points in the two images. Let  $P_s = \{f_s(x_i, y_i), i = 1, \dots, N_s\}$  and  $P_r = \{f_r(X_j, Y_j), j = 1, \dots, N_r\}$  be the set of feature points detected in the warp and reference images, respectively. Let  $T_c$  denote the threshold value above which two feature points are considered similar. The point  $f_r(X_k, Y_k)$  is considered the most similar feature point to  $f_s(x_l, y_l)$  if

$$C_{f_s, f_r}(x_l, y_l, X_k, Y_k) = \max_{1 \leq j \leq N_r} C_{f_s, f_r}(x_l, y_l, X_j, Y_j) \quad (18)$$

Therefore, the matching process is achieved in the following way. For each point  $f_s(x_l, y_l) \in P_s$ , all points  $f_r(X_j, Y_j) \in P_r$  are examined and the most similar point  $f_r(X_k, Y_k)$  is chosen. Next we test whether the achieved correlation is reasonably high.

If  $C_{f_s, f_r}(x_l, y_l, X_k, Y_k) > T_c$ , then  $f_r(X_k, Y_k)$  is called “the best match” of  $f_s(x_l, y_l)$ . To verify that the match is consistent in the reverse direction, we test whether the best match of  $f_r(X_k, Y_k)$  exists and is indeed given by  $f_s(x_l, y_l)$ . If that is the case, both points are taken as matched.

This reverse verification reduces the number of mismatched pairs in the matching process and allows for the use of smaller window sizes. Nevertheless, some false matches will inevitably occur. This initial part of the matching process is a crucial phase of the registration process. If the initial registration parameters are invalid the search for a registration transformation evolves in a wrong direction, and the correct trend may not be recovered in later steps. Therefore, a consistency-checking procedure is performed in order to eliminate incorrect matches and to improve registration precision.

Consistency-checking approaches were considered for use in the proposed algorithm. The first approach was similar to the one used in Li *et al.*, (1995), which is performed recursively in such a way that the most likely incorrect match is deleted first, followed by the next most likely incorrect match, and so on. This approach is based on the fact that distances are preserved under a rigid transformation. In order to handle the situation in which the deformation between the images is not rigid, we propose an alternative procedure. This is an empiric method that uses combinatorial search. Let be two pairs of control points  $P_k = \{X_k, Y_k, x_k, y_k\}$  and  $P_l = \{X_l, Y_l, x_l, y_l\}$ .

Let be  $D_{lk}$  and  $d_{lk}$  the Euclidian distances between the points  $P_k$  and  $P_l$  in the reference and adjust images, respectively:

$$D_{lk} = \sqrt{(X_l - X_k)^2 + (Y_l - Y_k)^2} \quad (19)$$

$$d_{lk} = \sqrt{(x_l - x_k)^2 + (y_l - y_k)^2}$$

Let  $E_{ij}$  a error measure that relates the Euclidean distances  $D_{ij}$  and  $d_{ij}$  between the control points  $P_i$  and  $P_j$ :

$$E_{ij} = \frac{D_{ij} - d_{ij}}{\min(D_{ij}, d_{ij})} \quad (20)$$

for  $i, j = 1, \dots, K$  and  $i \neq j$ . Let  $p$  the minimum number of control points necessary to calculate the parameters of the transformation function selected and  $T_e$  an error threshold. The outliers elimination procedure as follows:

- (i) Group the  $K$  control points pairs in the list of candidate pairs  $L_K$ , in sets of  $n = p + 1$  elements, denoted by  $C_i^n = \{P_1, P_2, \dots, P_n\}$ ,  $i = 1, \dots, \binom{K}{n}$ ;
- (ii) For each set  $C_i^n$ , calculate the error,  $E_i^n$ , using the control point pairs in the set;
- (iii) Select the set  $C_k^n$  with the least error  $E_k^n$ ;
- (iv) For every  $P_j \in L_K$  and  $P_j \notin C_k^n$ ,  $j = 1, \dots, K$  do:
  - Add a pair of control points  $P_j$  to the set  $C_k^n \cup C_{kj}^n$ ;
  - Calculate the set error for  $C_{kj}^n$ , denoted by  $E_{kj}^n$ ;
- (v) Select the set  $C_{k_j}^n$ , among all sets generated in the previous step, with the least error  $E_{k_j}^n$ ;
- (vi) if  $E_{k_j}^n > T_e$ , stop;
- (vii) Let  $C_k^n = C_{k_j}^n$ ;
- (viii) Go to step iv;

The possibility that the  $p + 1$  elements from initial set are wrong and even so present a small initial error exists. But, in this case, as points are added, the error tends to increase rapidly and, thus, one can detect the unfavorable situation interrupting the process and restarting it by choosing the next set with least error. In all tested cases in this work, this method was successful to perform consistency checking.

### 4.3 Image Warping

The above procedure provides a set of reliable matches which are used to determine a warping function that yields the best registration of the LL subbands at the precision available in level  $L$  of the wavelet transform.

To model the deformation between the images, a 2D affine transform with the parameters  $s, \theta, \Delta x, \Delta y$  is used (ZHENG and CHELLAPPA, 1993), such that

$$\begin{aligned} X &= T_1 x, y^a = s x \cos \theta^a + y \sin \theta^a + \Delta x \\ Y &= T_2 x, y^a = s x \sin \theta^a + y \cos \theta^a + \Delta y \end{aligned} \quad (21)$$

where  $x, y^a$  and  $X, Y$  are corresponding points in the warp and reference images, respectively. This model is commonly used in remote sensing applications and is a good approximation for images taken under similar imaging directions (Dana and Anandan, 1995), and which have been geometrically corrected (e.g. for Earth

curvature and rotation). In most remote sensing applications the images have a certain level of geometrical correction, which enables the use of this class of transformations.

### 4.4 Refinement

The point matching and image warping steps can be performed at progressively higher resolutions in a similar fashion to that described above. At each level  $l < L$ , the warp image  $f_s$  is transformed using the parameters estimated from the wavelet transform at the lower resolution level ( $l + 1$ ). In other words, the LL, LH, HL, and HH subbands at level  $l + 1$  are recombined to reconstruct the LL subband at level  $l$ , which is then warped by the transformation specified at the previous point matching operation.

Fig. 4 shows the block diagram of the steps involved in the registration refinement process. Let  $f_s^l$  denote the registered image. Registration refinement is achieved using the registered image and the set of feature points detected in the reference image. Each feature point  $f_r, X_k, Y_k$  detected in the image  $f_r$  at level  $l$  is matched to  $f_s^l, x_l, y_l$  if

$$\max_{\substack{m, n \in \mathbb{Z} \\ |m| \leq 2, |n| \leq 2}} C_{f_s^l f_r}(x_l + m, y_l + n, X_k, Y_k) = C_{f_s^l f_r}(x_l, y_l, X_k, Y_k) \quad (22)$$

where  $w_r$  is the width of the registration refinement window.

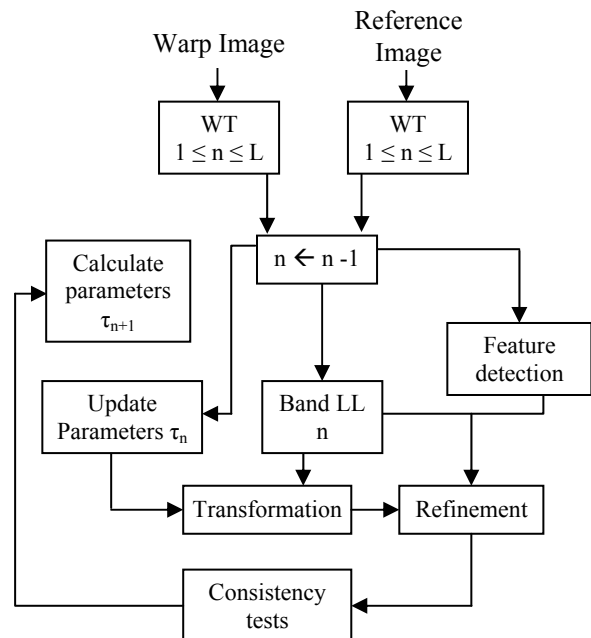


Fig. 4 – Registration refinement process.

The traditional measure of registration accuracy is the root mean square error (RMSE) between the matched points after the transformation, defined as

$$RMSE = \sqrt{\frac{1}{N} \sum_{i=1}^N (x_i - y_i)^2} \quad (23)$$

where  $N$  is the number of matched points. This measure is used as a criterion to eliminate earlier matches which are considered imprecise. Poor matches are sequentially eliminated in an iterative fashion until the  $RMSE$  value is lower than 0.5 pixel.

In the refinement process, the matching operation is performed only for those points, which fall on the overlapping region of the reference and warp images. This eliminates unnecessary computations and speeds up the procedure.

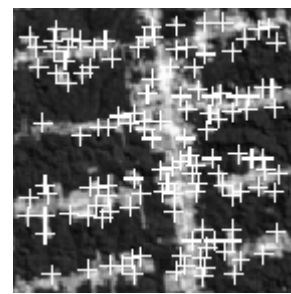
At each level the warping parameters are updated considering the parameters obtained in the previous level and in the refinement step. After processing all levels the final parameters are determined and used to warp the original warp image, thereby producing the final registration of the warp image with respect to the reference image.

## 5. EXPERIMENTAL RESULTS

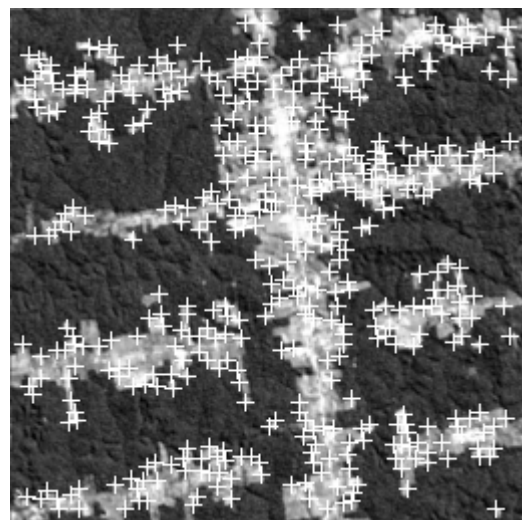
The feature extraction algorithm was tested for many types of images. Next, three experiments are presented. The images used in the experiments correspond to a forest region in Amazon (band 5), an urban area in the Brasilia city (band 4), and an agriculture region close to Agudos city (band 5), acquired by the satellite Landsat-TM5. The original images (512x512 pixels) were processed for two decomposition levels.

Figures 5, 6 and 7 show the distribution of point features superimposed on the band LL of the wavelet decomposition in the two resolution levels and on the original test images. The parameters used in all experiments were:  $\beta=3$  (to eliminate less significant features),  $T_w=0.95$  for the contrast threshold and a neighborhood  $V_p$  of 7x7 pixels in the local maxima selection process. These parameters values have been successfully tested for various images, which indicates the reliability of the method.

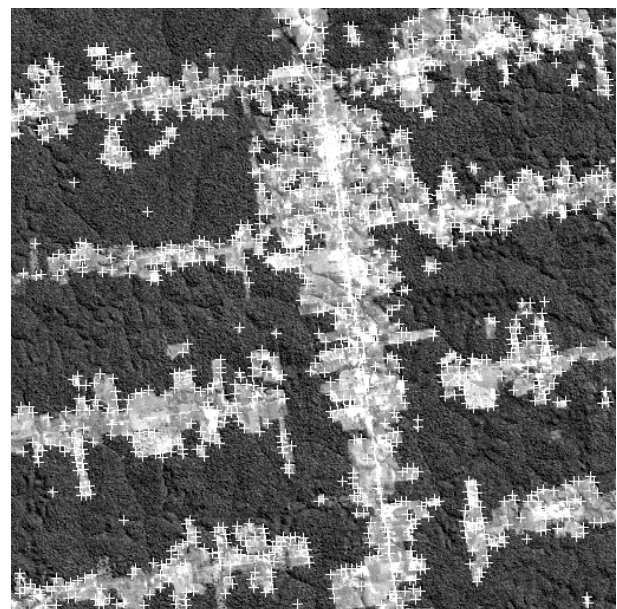
From this point on, we present some registration results of simulated images in order to show the performance of the registration algorithm proposed in this work. First, the images are artificially deformed using known transformation parameters (rotation, translation and scale). From this set of parameters we can calculate the actual required transformation to register the images. Next, the deformed images are transformed back (registered) using the proposed registration algorithm. This transformation process provides estimated parameters, which give very good approximations to the actual transformations used in the experiment, as seen in Table 2.



(a)

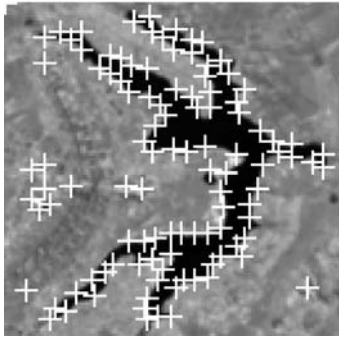


(b)

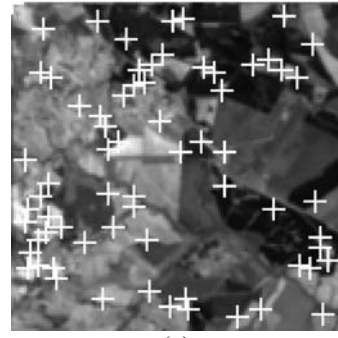


(c)

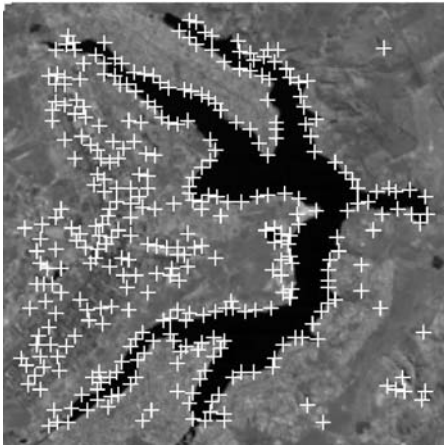
Fig. 5 – Selected feature points of a forest area, at resolution (a) 128x128, (b) 256x256, and (c) 512x512 pixels.



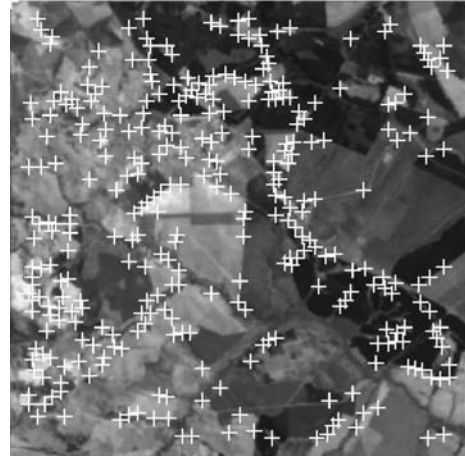
(a)



(a)



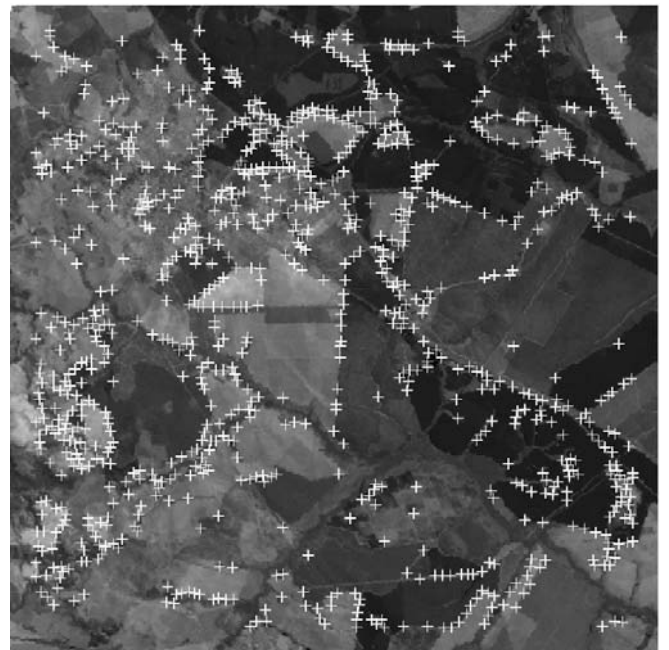
(b)



(b)



(c)



(c)

Fig. 6 – Selected feature points of an urban area (Brasilia), at resolution (a) 128x128, (b) 256x256, and (c) 512x512 pixels.

Fig. 7 – Selected feature points of an agriculture area (Agudos), at resolution (a) 128x128, (b) 256x256, and (c) 512x512 pixels.

For this experiment we selected 6 images of different regions and sensors. Figures 8(a)-(f) show the original images and Table 2 shows the distortion model parameters (actual and estimated transformations).

TABLE 2 – ACTUAL AND ESTIMATED DISTORTION PARAMETERS

Images	Area	Parameters	$s$	$\theta$	$\Delta x$	$\Delta y$
AES-1 (radar)	agric/forest 600×600	actual	1.1	9.0	100.0	70.0
		estimated	1.1	8.99	99.68	69.97
aerial photograph	urban 600×600	actual	1.0	-12.0	-100.0	-50.0
		estimated	1.0	-12.0	-100.1	-49.92
SIR-C (radar)	agricultural 512×512	actual	0.92	8.0	80.0	-20.0
		estimated	0.919	8.0	79.97	-19.92
optical sens (balloon)	desert 512×512	actual	0.90	15.0	38.0	-55.0
		estimated	0.90	14.99	37.98	-54.97
LandsatTM	forest 1000×1000	actual	1.10	20.0	45.0	-100.0
		estimated	1.10	20.01	45.12	-100.1
SPOT	vegetation 1000×1000	actual	0.95	10.30	385.0	201.0
		estimated	0.95	10.29	384.56	200.63

Fig. 8(a) is a radar image AES-1 (Aerosensing Radarsystems, Germany) of an agriculture and forest area in Wessling region, band X, 600B 600 pixels, resampled for 2 meter pixel size (original resolution = 0.5 m). Shown in Fig. 8(b) is an aerial photograph of the city of São José dos Campos, SP, Brazil, 600B 600 pixels, taken on 04/08/1976. A radar image SIR-C/X-SAR (Spaceborne Imaging Radar C/X-Band Synthetic Aperture Radar) acquired on 04/13/1994 from the Space Shuttle of the Bebedouro region, in Pernambuco, Brazil, band L, polarization HH, pixel = 12.5 meters, 512B 512 pixels, is illustrated in Fig. 8(c). Fig. 8(d) shows a balloon image of the Mojave Desert taken with a CCD camera. Fig. 8(e) shows a Landsat-TM image, band 3, 1000B 1000 pixels, acquired in August/1991 of the Manaus region, in Amazon, Brazil. Fig. 8(f) shows an image of Brasília, DF, Brazil, with a gallery forest (forest along alluvial areas) and savannah, acquired in 1989 by the SPOT satellite, panchromatic band (resolution 10 meters), 1000B 1000 pixels.

The images were transformed using the similarity model with the following parameters: scale ( $s$ ), rotation ( $\theta$ ) and translation ( $\Delta x$  and  $\Delta y$ ). Table 2 shows the types of images, as well as the distortion model parameters used for image simulation and the parameters estimated by the proposed method. In this table, the measurement units are degree ( $\theta$ ) and pixels ( $\Delta x$  and  $\Delta y$ ). One can observe that the estimated parameters are very similar to the real parameters even in Experiment 5 where the rotation is relatively high ( $\theta = 20$  degrees). The algorithm parameters were the same for all tests:  $w_c = 13$ ,  $T_c = 0.75$  and  $T_w = 0.9$ . Values for  $\beta$  were adjusted in order to generate a sufficiently large number of initial control points, leading to a successful registration procedure. The images were processed in  $L = 3$  (1000B 1000) and in  $L = 2$  (400B 400) resolution levels.

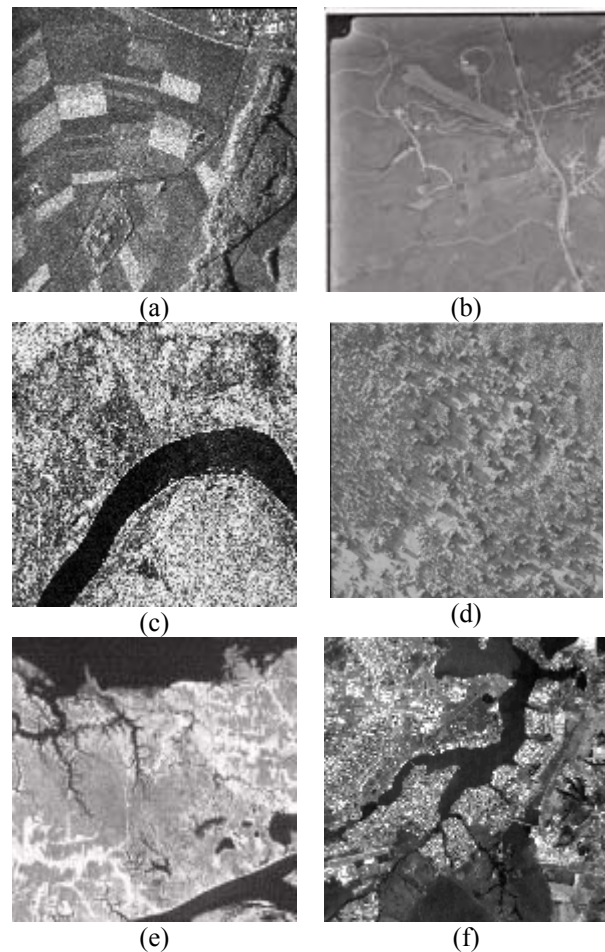


Fig. 8 – Images used to simulate the deformed images: (a) radar image AES-1, band X (600B 600), agricultural/forest area; (b) aerial photograph of São José dos Campos (600B 600); (c) radar image SIR-C/X, band L, agricultural area (512B 512); (d) Mojave Desert, acquired with a CCD camera (512B 512); (e) Landsat-TM image of forest area in Manaus (1000B 1000) and (f) SPOT image of Brasília, DF, panchromatic band (10 m), (1000B 1000).

To illustrate the performance of our algorithm, some results obtained in the image simulation and correction processes are presented in Figures 9-11. The figures show the initial control points superimposed on reference and simulated images, with parameters of Table 2, in the lowest level of resolution.

Therefore, to test the registration method and demonstrate its feasibility for real applications, some experiments were performed. An important project at INPE is the study of land use in the Amazonia region (Alves et al., 1994). In this project the image registration task is performed manually with high computational cost. Due to the textural and multi-temporal characteristics of forest images, automatic registration techniques based on closed contours as that one proposed by Li et al. (1995) do not always work properly.

Therefore, the algorithm was tested to register multi-temporal images of forest, agriculture and urban areas obtained by the SPOT-3, Landsat-5 and JERS-1

satellites (Table 3). The image sizes are 512B 512 pixels and they were taken at different times. The algorithm parameters were the same for all tests:  $\beta=3$ ,  $w_c=13$ ,  $T_c=0.75$  and  $T_w=0.9$ . The images were processed in  $L=2$  resolution levels. Before registration, the radar images were filtered (using a gamma filter) to reduce speckle noise (Oliver and Quegan, 1998).

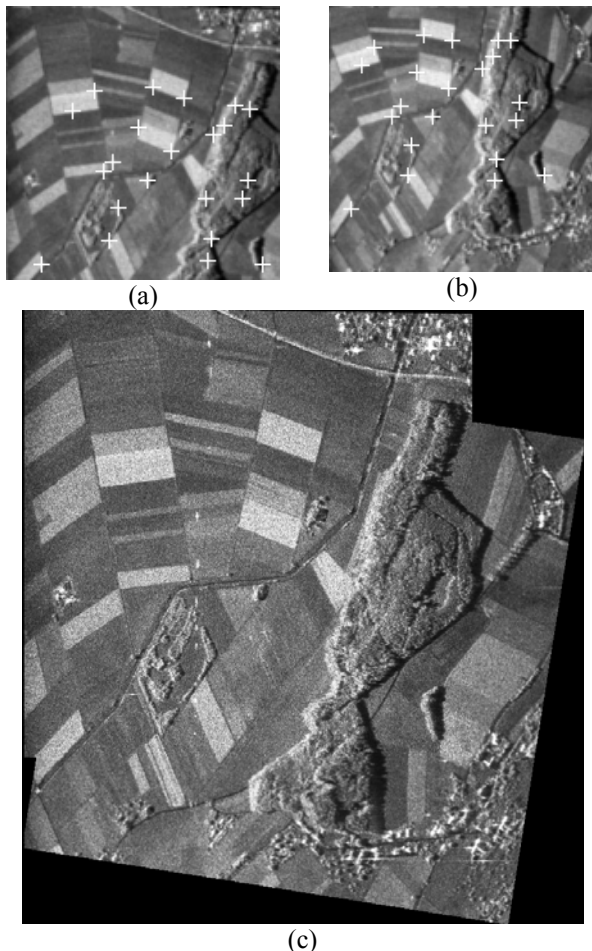


Fig. 9 – Initial control points superimposed on (a) reference and (b) simulated images (AES-1) in the lowest level of resolution and (c) Mosaic after registering ( $L=2$ ,  $\beta=1$ ).

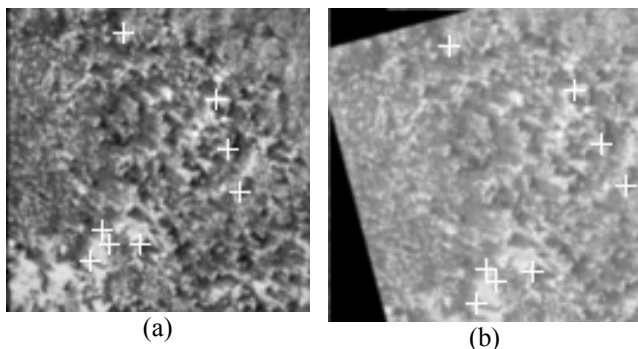


Fig. 10 – Initial control points superimposed on (a) reference and (b) simulated images (Mojav desert) in the lowest level of resolution ( $L=2$ ,  $\beta=1$ ).

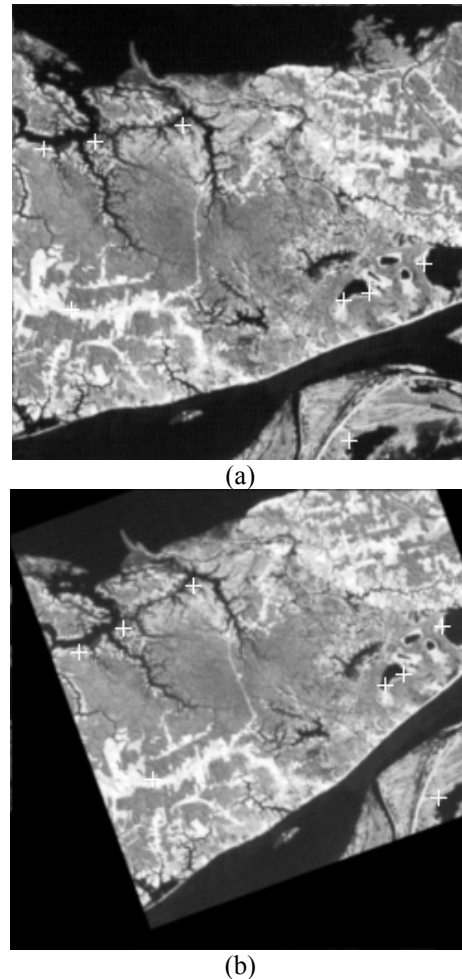
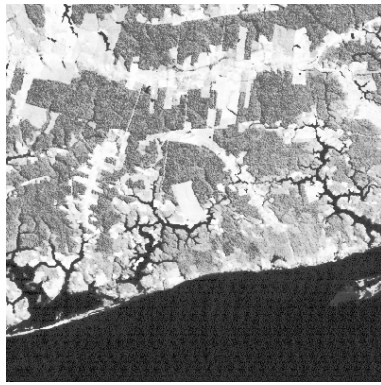


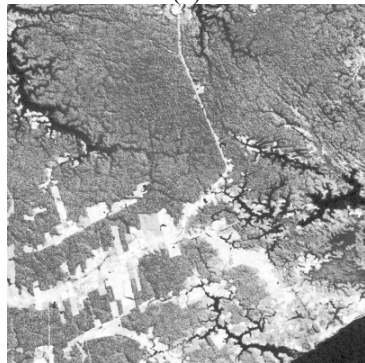
Fig. 11– Initial control points superimposed on (a) original and (b) simulated images (forest) in the lowest level of resolution ( $L=2$ ,  $\beta=2$ ).

TABLE 3 – TEST IMAGES

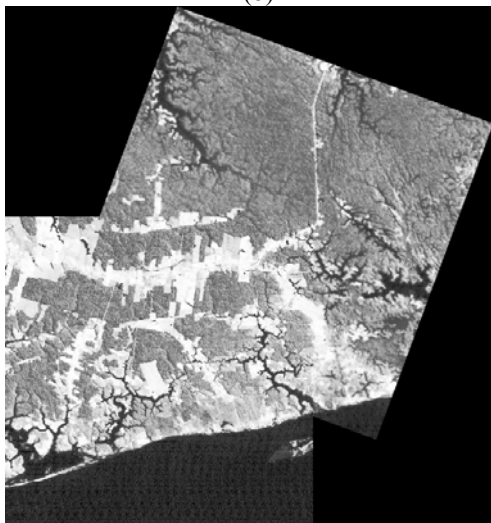
Images	Region	Satellite	Band	Date	# PCs	RMSE (pixel)
TM925AM TM945AM	Amazon	Landsat-TM Landsat-TM	5 5	07/06/92 15/07/94	169	0.787
TM975AM TM955AM	Amazon	Landsat-TM Landsat-TM	5 5	07/07/97 03/08/95	485	0.655
TM965AM TM945AM	Amazon	Landsat-TM Landsat-TM	5 5	20/07/96 15/07/94	326	0.828
TM905IT TM945IT	Itapeva	Landsat-TM Landsat-TM	5 5	09/09/90 18/07/94	184	0.989
TM905IT TM945RIT	Itapeva	Landsat-TM Landsat-TM	5 5	09/09/90 18/07/94	287	0.828
TM945AG TM925AG	Agudos	Landsat-TM Landsat-TM	5 5	09/07/94 21/09/92	294	0.344
SP953SP TM944SP	S. Paulo	SPOT Landsat-TM	3 4	08/08/95 07/06/94	267	0.434
SP953DF TM944DF	Brasilia	SPOT Landsat-TM	3 4	08/08/95 07/06/94	110	0.915
JERS93 JERS96	Amazon	JERS-1 JERS-1	X X	26/06/93 13/08/96	153	1.101
JERS93 JERS95	Amazon	JERS-1 JERS-1	X X	26/06/93 10/10/95	79	0.669



(a)



(b)

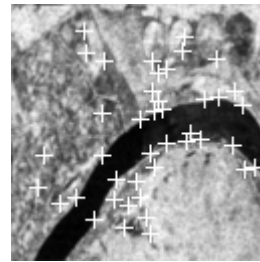


(c)

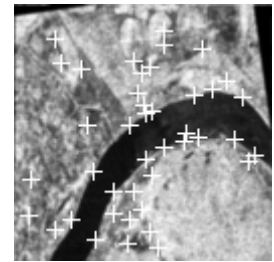
Fig. 12 – Mosaic between original and simulated Landsat images, after correction: (a) reference image (400x400 pixels); (b) simulated image and (d) Mosaic after registering ( $L=2$ ,  $\beta=3$ ).

Figures 14-18 show some registration results. Fig. 14 shows the registration of Amazon tropical forest images taken from the TM5 sensor (T2). These images were successfully registered with 485 control points. Fig. 15 shows the registration of two images from the urban area of São Paulo. A SPOT image, band 3 was reduced to 30 @meter pixel size and registered with Landsat-TM5 image, band 4. Fig. 16 shows the registration of Amazon region images taken from the TM5 sensor, band 5, in different dates. Fig. 17 shows the registration of Amazon region images taken from

JERS-1. Finally, Fig. 18 shows the registration of an urnab region images (Brasilia) taken from SPOT and Landsat-TM systems.



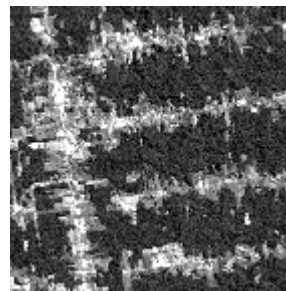
(a)



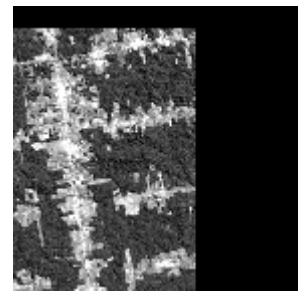
(b)

Fig. 13 – Initial control points superimposed on (a) reference and (b) simulated images (SIR-C/X) in the lowest level of resolution ( $L=2$ ,  $\beta=2$ ).

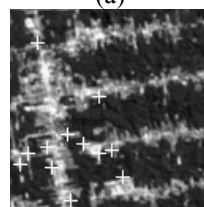
Although most of the images used in this work have similar spectral bands, seasonality differences present in these images make it difficult for the automatic registration process. Before registration, images can be preprocessed in order to improve their contrast and to reduce noise.



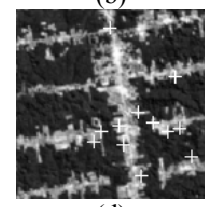
(a)



(b)



(c)



(d)

Fig. 14 – Images of Amazon region: (a) reference image (TM925AM); (b) Registered image (TM945AM); (c) and (d) show initial control points superimposed on reference and warp images in the lowest level of resolution.

Also, some images were enhanced to improve their visual quality or filtered to reduce the speckle noise. Moreover, some other experiments with images from urban, forest and agricultural areas were performed and in all cases we obtained encouraging results.

In order to measure the registration error, we used the root mean square error (*RMSE*) defined in Equation 23. Control points different from those identified in the registration process (called test points) were manually chosen. Given the spatial transformation and the test points, the error was calculated for each pair

of images. The results are shown in the last column of Table 3. We find that, in most cases, the registration error is less one pixel, indicating good registration accuracy.

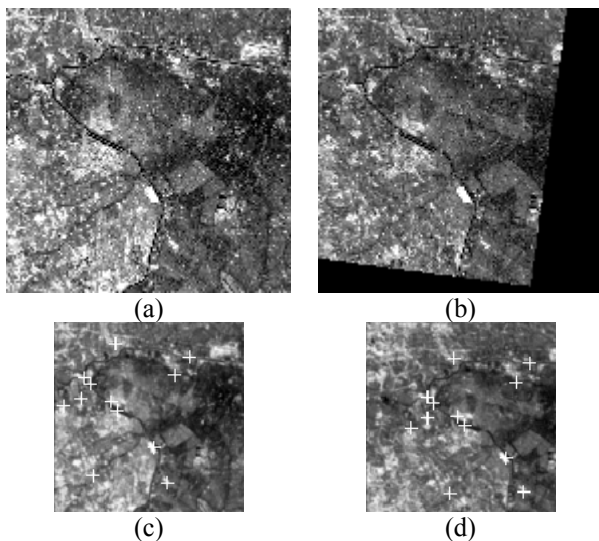


Fig. 15 – Images of urban area: (a) reference image (TM944SP); (b) Registered image (SP953SP); (c) and (d) show initial control points superimposed on reference and warp images in the lowest level of resolution.

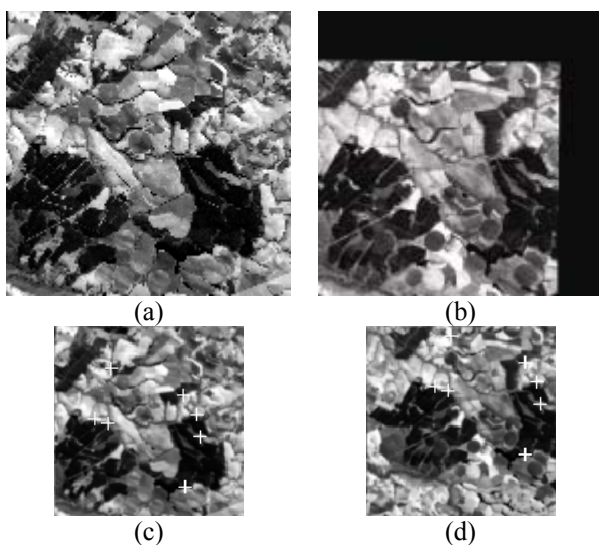


Fig. 16 – Images of Agriculture area: (a) reference image (TM945I); (b) Registered image (TM905I); (c) and (d) show initial control points superimposed on reference and warp images in the lowest level of resolution.

To investigate the *RMSE* behavior with different levels of wavelet decomposition the following experiment was performed. A Landsat-TM image of the Amazon region (3354B4096 pixels, band 5) was selected and warped by a similarity transformation with parameters  $s = 0.90$ ;  $\theta = 10$ ;  $\Delta x = 200$  and  $\Delta y = @400$ .

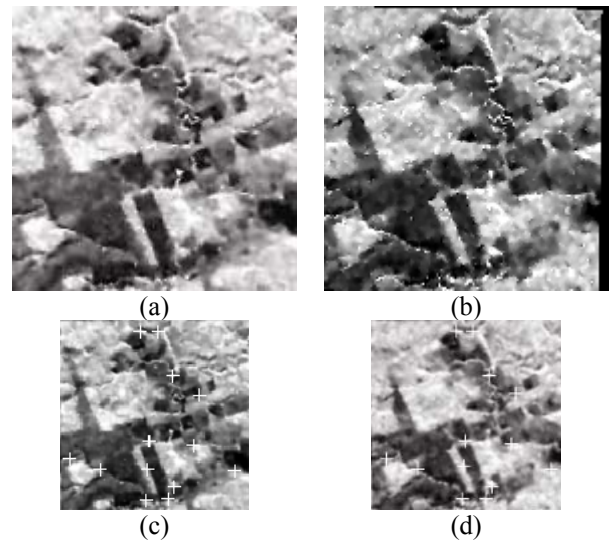


Fig. 17 – Registering JERS93 and JERS96 images:(a) reference image (JERS93); (b) registered image (JERS96); (c) and (d) show the initial control points superimposed on reference and warp images in the lowest level of resolution.

The original and warped images were decomposed by wavelet transforms in 7 levels of resolution ( $L=0, \dots, 6$ ). The graph in Fig. 13 shows the refinement of TM95 and TM97 images along the various levels of resolution, starting with  $L=6$  until  $L=0$ . At the coarsest level of resolution, the registration transformation is estimated with low precision. As the resolution increases (i.e., as  $L$  decreases) the registration transformation is progressively refined until the registration process is completed.

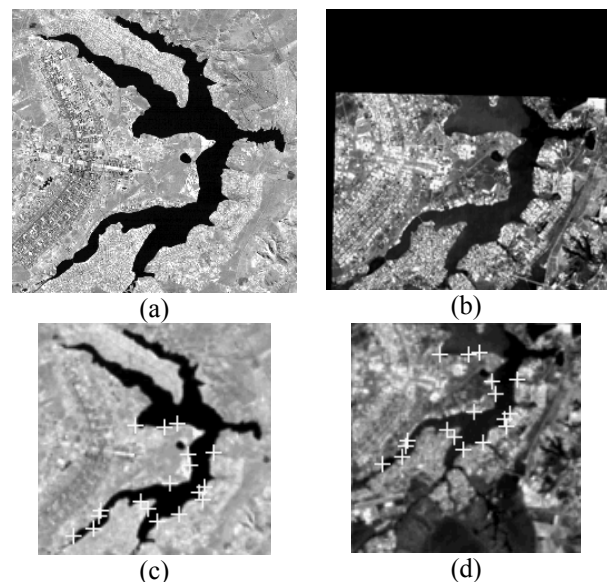


Fig. 18 – Images of urban area: (a) reference image (TM944SP); (b) Registered image (SP953SP); (c) and (d) show initial control points superimposed on reference and warp images in the lowest level of resolution.

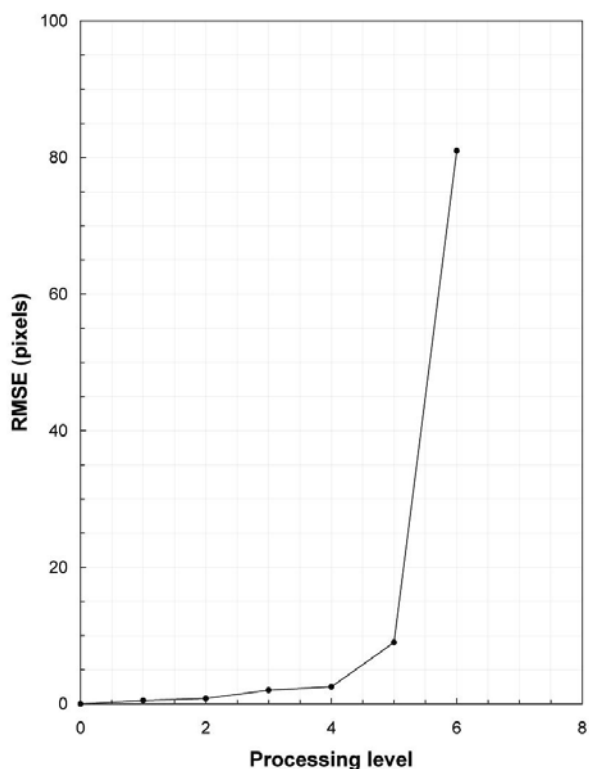


Fig. 19 – Registration error (RMSE) in different resolution levels (L=6), for Landsat-TM5 images.

## REFERENCES

ALVES, D. S.; MEIRA FILHO, L. G.; ALGE, J. C. L.; MELLO, E. K.; MOREIRA, J. C.; MEDEIROS, J. S. The Amazonia Information System. **International Symposium on Photogrammetry and Remote Sensing**, v. 7, p. 259–266, 1992.

BARNEA, D. I.; SILVERMAN, H. F. A class of algorithms for fast digital image registration. **IEEE Transactions on Computers**, v. 21, n. 2, p. 179–186, 1972.

BIJAOU, A.; GIUDICELLI, M. Optimal image addition using the Wavelet Transform. **Experimental Astronomy**, Springer, v. 1, n. 6, p. 347–363, 1991.

BRUNELLI, R.; MESSELODI, S. Robust estimation of correlation with applications to computer vision. **Pattern Recognition**, v. 28, n. 6, p. 833–841, June 1995.

CHEONG, C.; AIZAWA, K.; SAITO, T.; HATORI, M. Subband image coding with biorthonormal wavelets. **EICE Transactions Fundamentals of Eletronics, Communications and Computer Sciences**, E75-A, p. 871–881, 1992.

CHUI, C. **An introduction to wavelets**. Academic Press, 1992.

## 6. CONCLUSIONS

A multiresolution approach has been successfully applied to two steps of the image registration process: feature identification and matching. The registration method presented here is very simple and easy to apply. A significant amount of computation is saved in comparison to traditional pixel-by-pixel searching methods because the matching is carried out only on the selected feature points and in a coarse-to-fine manner.

Due to the fact that the registration procedure uses the gray level information content of the images in the feature matching process, it is more appropriate to register images of the same sensor or with similar spectral bands. Nevertheless, it has demonstrated good performance for many images of forest, urban and agricultural areas from Landsat-TM and SPOT sensors taken at different times.

## ACKNOWLEDGEMENTS

The authors would like to thank Dr. Diógenes S. Alves for providing the Amazon region images, Mr. Sergio D. Faria, for providing the agriculture images, José Mura and Luciano Dutra for providing radar images, and finally Dr. Manjunath for providing Mojav Desert images.

COLE-RHODES, A.A.; JOHNSON, K.L.; LE MOIGNE, J.; ZAVORIN, I. Multiresolution registration of remote sensing imagery by optimization of mutual information using a stochastic gradient. **IEEE Transactions on Image Processing**, v. 12, n. 12, p. 1495–1511, Dec. 2003.

CORVI, M.; NICCHIOTTI, G. Multiresolution image registration. **Proceedings, International Conference on Image Processing**, v. 3, p. 224–227,

DANA, K. J.; ANANDAN, P. Registration of visible and infrared images. **Proceedings of the SPIE Conference on Architecture, Hardware and Forward-Looking Infrared Issues in Automatic Target Recognition**, v. 1957, p. 1–12, 1995.

DARE, P.; DOWMAN, I. An improved model for automatic feature-based registration of SAR and SPOT images. **ISPRS Journal of Photogrammetry and Remote Sensing**, Elsevier Science, v. 56, n. 1, p. 13–28, 2001.

DJAMDJI, J. P.; BIJAOU, A. Disparity analysis: a wavelet transform approach. **IEEE Transactions on Geoscience and Remote Sensing**, v. 33, n. 1, p. 67–76, Jan. 1995.

DJAMDJI, J. P.; BIJAOU, A.; MANIERE, R. Geometrical registration of images: the multiresolution

- approach. **Photogrammetric engineering and remote sensing, American Society for Photogrammetry and Remote Sensing**, v. 59, n. 5, p. 645–653, 1993.
- FEDOROV, D.; FONSECA, L. M. G.; COSTA, M. H.; MANJUNATH, B. S. AND KENNY, C. Automatic registration and mosaicking system for remotely sensed imagery. **9th International Symposium on Remote Sensing**, p. 22–27, 2002.
- FLIEGE, N. J. **Multirate Digital Signal Processing: Multirate Systems, Filter Banks, Wavelets**. John Wiley & Sons, Inc. New York, NY, USA, 1994.
- FONSECA, L. M. G.; COSTA, M. H.; MANJUNATH, B. S. AND KENNY, C. Automatic registration of satellite imagery. **Greenbelt: NASA Goddard Space Flight Center**, p. 13–27. 1998.
- FONSECA, L. M. G.; COSTA, M. H. M. Automatic registration of satellite images. **X Brazilian Symposium on Computer Graphics and Image Processing**, p. 219–226. 1997.
- FONSECA, L. M. G. and MANJUNATH, B. S. Registration techniques for multisensor remotely sensed imagery. **Photogrammetric engineering and remote sensing, American Society for Photogrammetry and Remote Sensing**, v. 62, n. 9, p. 1049–1056, 1996.
- FOOKES, C.; MAEDER, A.; SRIDHARAN, S.; COOK, J. Multi-Spectral Stereo Image Matching using Mutual Information. **3D Data Processing, Visualization and Transmission**, p. 961-968, 2004.
- GONZALEZ, R. C.; WOODS, R. E. **Digital image processing**. Addison-Wesley Reading, Mass, 1992.
- GOVINDU, V.; SHEKHAR, C.; CHELLAPPA, R. Using geometric properties for correspondence-less image alignment. **Fourteenth International Conference on Pattern Recognition**, v. 1, 1998.
- GRAPS, A. An introduction to wavelets. **IEEE Computational Science and Engineering**, v. 2, n. 2, p. 50–61, 1995.
- HSIEH, J. W.; LIAO, H.M.; FAN,K.C.; KO, M.T.; HUNG.Y.P. Image registration using a new edge-based approach. **Computer Vision and Image Understanding**, Elsevier Science Inc. New York, NY, USA, v. 67, n. 2, p. 112–130, 1997.
- KANADE, T.; OKUTOMI, M. A Stereo Matching Algorithm with an Adaptive Window: Theory and Experiment. **IEEE Transitions in Pattern Analysis**. Mach. p. 920–932. 1994.
- KENNEY, C.; MAJUNATH, B. S. **Point Matching for Registration with Fit Assessment**. *To be published*. 2001.
- KHOSRAVI, M.; SCHAFFER, R. Template matching based on a grayscale hit-or-miss transform. **IEEE Transactions on Image Processing**, v. 5, n. 6, p. 1060–1066, 1996.
- LI, H.; MANJUNATH, B. S.; MITRA, S. K. A contour-based approach to multisensor image registration. **IEEE Transactions on Image Processing**, v. 4, n. 3, p. 320–334, 1995.
- MALLAT, S. G. **A Wavelet Tour of Signal Processing**. Academic Press, 1999.
- MALLAT, S.; HWANG, W. L. Singularity detection and processing with wavelets. **IEEE Transactions on Information Theory**, v. 38, n. 2, p. 617–643, March 1992.
- MALLAT, S.; ZHONG, S. Characterization of signals from multiscale edges. **IEEE Transactions on Pattern Analysis and Machine Intelligence**, v. 14, n. 7, p. 710–732, 1992.
- MALLAT, S. G.; ZHONG, S. **Wavelet maxima representation – Wavelets and Applications**, Springer-Verlag, 1991.
- MALLAT, S. A Theory for Multiresolution Signal Decomposition: The Wavelet Representation. **IEEE Transactions on Pattern Analysis and Machine Intelligence**, v. 11, n. 7, p. 674–693, 1989.
- MALLAT, S. G. Multifrequency channel decompositions of images and wavelet models. **IEEE Transactions on Acoustics, Speech, and Signal Processing**, v. 37, n. 12, p. 2091–2110, 1989.
- MOIGNE, J. L. Parallel registration of multi-sensor remotely sensed imagery using wavelet coefficients. **The International Society for Optical Engineering (SPIE)**, v. 2242, p. 432–443, 1994.
- OLIVER, C.; QUEGAN, S. **Understanding Synthetic Aperture Radar Images**. Artech House Boston, 1998.
- PRATT, W. K. Correlation techniques of image registration. **IEEE Transactions on Aerospace and Electronic Systems**, AES-10, n. 3, p. 353–358, May 1974.
- ZHENG, Q.; CHELLAPPA, R. A computational vision approach to image registration. **IEEE Transactions on Image Processing**, v. 2, n. 3, p. 311–326, 1993.
- ZITOVA, B.; FLUSSER, J. Image registration methods: a survey. **Image and Vision Computing, Elsevier Science**, v. 21, n. 11, p. 977–1000, 2003.